ROYAL SOCIETY OF CHEMISTRY

PAPER

Check for updates

Examining intermolecular interactions in crystal structures of amide-substituted 2-aminopyrimidine derivatives†

Aloka A. Marasinghe, Boris B. Averkiev and Christer B. Aakeröy [iD] *

A systematic structural investigation of acetylated 2-aminopyrimidine derivatives was conducted to understand the balance between hydrogen and halogen bonds in supramolecular assembly. The 2-aminopyrimidine derivatives were grouped into three series to examine the effects of alkyl chain length, chain nature, and halogen substitution on supramolecular assembly. A total of twenty-one new crystal structures across these targets indicate that steric effects (alkyl chain length), the nature of the carbon chain, and halogen-atom substitution did not influence the assembly, with primary bonding motifs remaining largely consistent within each series. Notably, the study demonstrated that hydrogen bonds could be replaced by halogen bonds without disrupting overall crystal assembly when the halogen bond donor was sufficiently strong. Analysis of bond directionality illustrated that halogen bonds are more directional than hydrogen bonds, with hydrogen bond angles ranging from 126° to 166°, chlorine halogen bonds from 170° to 175°, and bromine halogen bonds from 168° to 177°. These findings highlight the potential of halogen bonds as reliable alternatives to hydrogen bonding in crystal engineering and expand possibilities for designing molecular structures with tailored noncovalent interactions.

Introduction

Hydrogen bonding is recognized as a crucial force for directing molecular organizations and self-assembly,[1–5] with extraordinary impacts on biological systems as well as in materials science. More recently, halogen[6–10] and chalcogen[10–15] bonds have also gained considerable attention due to their ability to organize individual molecular building blocks into supramolecular assemblies with precise metrics and configurations. Even though these forces are well understood, it can still be challenging to predict the bulk structural outcome involving molecules that present multiple interaction sites within a single framework.[16–18] As a result, even relatively simple and rigid molecules can produce drastically different assemblies in the solid state, which creates a considerable hurdle for supramolecular synthesis and bottom-up design of desirable architectures.[19–24]

The way molecules are packed into crystalline lattices defines many of their bulk physical properties, and the field of crystal engineering has for many decades sought to gain more insight into how to navigate from molecules *via* intermolecular forces to form and function.[25–29] Progress in

this arena can positively impact the pharmaceutical[30–32] and agrochemical[33–36] industries, explosives,[37–41] and other advanced materials.[42,43] In addition, an improved understanding of interactions between individual components can also help to develop effective synthetic strategies for co-crystallization.[44–50] Consequently, there is a need for systematic structural studies on closely related compounds in order to elucidate how the balance between competing intermolecular forces can be harnessed.

It has been shown that calculated molecular electrostatic potentials (MEP) can provide valuable insights when it comes to rationalizing preferred binding patterns of functional groups and small molecules.[51–53] Often, the stronger acceptor sites (regions with large negative MEP) interact with the stronger donor sites (regions with large positive MEP). However, this is not always the case, as systems with multiple donor and acceptor sites, sterics, and other environmental factors can result in alternative supramolecular assemblies. To learn more about how the structural outcomes of small-molecule crystallization can be understood and rationalized, we have carried out a systematic structural investigation of three distinct series of amide-substituted 2-aminopyrimidine derivatives that present multiple donor and acceptor sites.

The 2-aminopyrimidine moiety was selected because it is a significant presence in numerous FDA-approved pharmaceutical drugs,[54–57] while the parent pyrimidine moiety ranks as the 10th most common aromatic moiety,[56]

Department of Chemistry, Kansas State University, Manhattan, KS, 66506, USA.
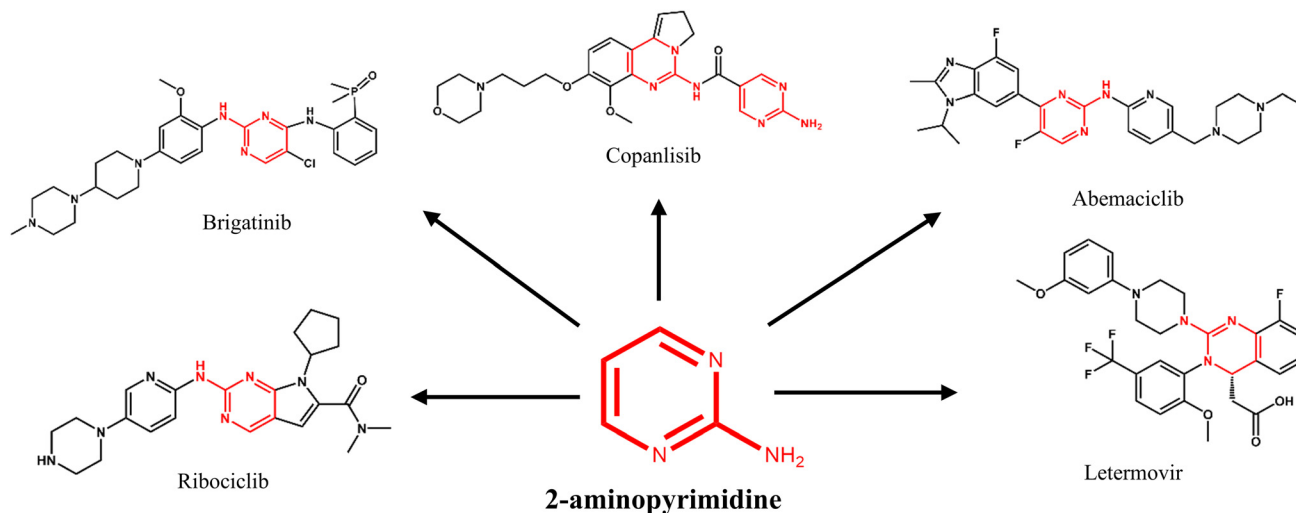*E-mail: aakeroy@ksu.edu*

Fig. 1 Some FDA-approved pharmaceutical drugs with 2-aminopyrimidine moieties.

Fig. 1. Furthermore, this 2-aminopyrimidine moiety is associated with several important biological properties such as antitumor, antimicrobial, antiviral, antithrombotic, antiparasitic activity, *etc.*[58–62]

Although these 2-aminopyrimidine derivatives have a broad spectrum of therapeutic activities they also face challenges as a result of sub-optimal properties such as thermal stability, solubility, bioavailability issues, *etc.* Therefore, additional examinations of their structural landscape are required.

In this study, we have synthesized and structurally characterized 21 molecules grouped into three series (**PM**, **Cl-PM**, and **Br-PM**) with different alkyl chain lengths, Fig. 2. We examined the crystal structures of these derivatives, addressing several key questions, such as whether the length of the alkyl chain(–R) affects the supramolecular self-assembly and whether the chain's specific nature (having an odd or even number of carbon) impacts the crystal structures. Additionally, we explore how these molecules behave in the solid state in the presence of an unequal number of hydrogen bond donors/ acceptors. We also examine the balance between the structure-directing effects of hydrogen bonds and halogen bonds. Finally, we attempt to identify any motif-building hydrogen-bond preferences among a series of postulated motifs Fig. 3.
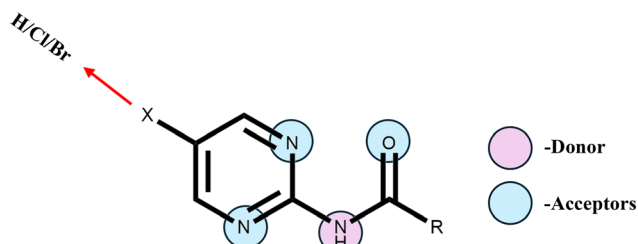

Fig. 2 Potential hydrogen bond donor–acceptor sites (R = methyl, ethyl, propyl, butyl, pentyl, hexyl, and heptyl).

Experimental section

All precursors and solvents were purchased commercially and used without further purification. ^{1}H NMR and ^{13}C NMR spectra were recorded on a Bruker 400 Hz and 600 Hz spectrometers. Melting points were recorded on a TA Instruments DSC Q20 differential scanning calorimeter. IR spectra were recorded with a Nicolet 380 FT-IR spectrometer using an attenuated total reflection (ATR) technique and ZnSe as the crystal.

All three series were synthesized according to an available literature procedure.[63]

PM series

Synthesis of *N*-(pyrimidin-2-yl)acetamide (PM-methyl). A solution of 2-aminopyrimidine (1.00 g, 11.00 mmol) in acetic anhydride (1.99 mL, 22.00 mmol) was stirred for 1.5 h at 100 °C and then cooled to 0 °C. The precipitate that formed was filtered off, and the reaction contents were extracted from ethyl acetate. The organic layer was washed with saturated sodium bicarbonate solution, brine, and water, dried with anhydrous magnesium sulfate, filtered, and concentrated *in vacuo* to isolate the pure product. Yield: 81.54%, Mp: 145–147 °C. ^{1}H NMR (400 MHz, DMSO-d$_6$): δ 10.52 (s, 1H), 8.64 (d, 2H), 7.15 (t, 1H), 2.19 (s, 3H). ^{13}C NMR (101 MHz, DMSO-d$_6$): δ 169.48, 158.76, 158.17, 116.97, 25.08.

Synthesis of *N*-(pyrimidin-2-yl)propionamide (PM-ethyl). A solution of 2-aminopyrimidine (1.00 g, 11.00 mmol) in propionic anhydride (2.68 mL, 22.00 mmol) was stirred for 1.5 h at 100 °C and then cooled to 0 °C. The precipitate that formed was filtered off, and the reaction contents were extracted using ethyl acetate. The organic layer was washed with saturated sodium bicarbonate solution, brine, and water, dried with anhydrous magnesium sulfate, filtered, and concentrated *in vacuo* to isolate the pure product. Yield: 82.39%, Mp: 126–128 °C. ^{1}H NMR (400 MHz, DMSO-d$_6$): 10.47 (s, 1H), 8.64 (d, 2H), 7.15 (t, 1H), 2.50 (q, 2H), 1.05 (t,
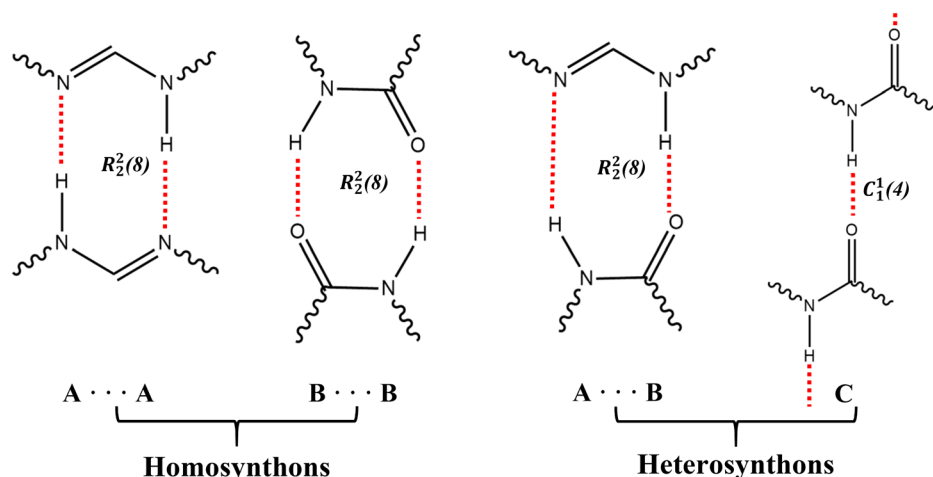
Fig. 3 Postulated primary hydrogen bond motifs.

3H). ^{13}C NMR (101 MHz, DMSO-d$_6$): δ 172.83, 158.75, 158.21, 116.93, 30.14, 9.65.

Synthesis of *N*-(pyrimidin-2-yl)butyramide (PM-propyl). A solution of 2-aminopyrimidine (0.50 g, 5.26 mmol) in butyric anhydride (1.66 mL, 10.52 mmol) was stirred for 1.5 h at 100 °C and then cooled to 0 °C. The precipitate that formed was filtered off, and the reaction contents were extracted from ethyl acetate. The organic layer was washed with saturated sodium bicarbonate solution, brine, and water, dried with anhydrous magnesium sulfate, filtered, and concentrated *in vacuo* to isolate the pure product. Yield: 81.84%, Mp: 102–104 °C. ^{1}H NMR (400 MHz, DMSO-d$_6$): δ 10.48 (s, 1H), 8.64 (d, 2H), 7.16 (t, 1H), 2.46 (t, 2H), 1.59 (h, 2H), 0.91 (t, 3H). ^{13}C NMR (101 MHz, DMSO-d$_6$): δ 171.88, 158.74, 158.17, 116.98, 38.73, 18.57, 14.07.

Synthesis of *N*-(pyrimidin-2-yl)pentanamide (PM-butyl). A solution of 2-aminopyrimidine (0.50 g, 5.26 mmol) in pentanoic anhydride (2.11 mL, 10.52 mmol) was stirred for 1.5 h at 100 °C and then cooled to 0 °C. The precipitate that formed was filtered off, and the reaction contents were extracted from ethyl acetate. The organic layer was washed with saturated sodium bicarbonate solution, brine, and water, dried with anhydrous magnesium sulfate, filtered, and concentrated *in vacuo* to isolate the pure product. Yield: 76.37%, Mp: 106–108 °C. ^{1}H NMR (400 MHz, DMSO-d$_6$): δ 10.48 (s, 1H), 8.64 (d, 2H), 7.15 (t, 1H), 2.48 (t, 2H), 1.53 (m, 2H), 1.31 (m, 2H), 0.89 (t, 3H). ^{13}C NMR (101 MHz, DMSO-d$_6$): δ 172.02, 158.74, 158.17, 116.99, 36.53, 27.31, 22.23, 14.23.

Synthesis of *N*-(pyrimidin-2-yl)hexanamide (PM-pentyl). A solution of 2-aminopyrimidine (0.50 g, 5.26 mmol) in hexanoic anhydride (2.43 mL, 10.52 mmol) was stirred for 1.5 h at 100 °C and then cooled to 0 °C. The precipitate that formed was filtered off, and the reaction contents were extracted from ethyl acetate. The organic layer was washed with saturated sodium bicarbonate solution, brine, and water, dried with anhydrous magnesium sulfate, filtered, and concentrated *in vacuo* to isolate the pure product. Yield:

86.53%, Mp: 110–112 °C. ^{1}H NMR (400 MHz, DMSO-d$_6$): δ 10.48 (s, 1H), 8.64 (d, 2H), 7.15 (t, 1H), 2.47 (t, 2H), 1.57 (p, 2H), 1.29 (m, 2H), 0.86 (t, 3H). ^{13}C NMR (101 MHz, DMSO-d$_6$): δ 172.02, 158.74, 158.18, 116.99, 36.78, 31.32, 24.85, 22.38, 14.33.

Synthesis of *N*-(pyrimidin-2-yl)heptanamide (PM-hexyl). A solution of 2-aminopyrimidine (0.50 g, 5.26 mmol) in heptanoic anhydride (2.77 mL, 10.52 mmol) was stirred for 1.5 h at 100 °C and then cooled to 0 °C. The precipitate that formed was filtered off, and the reaction contents were extracted from ethyl acetate. The organic layer was washed with saturated sodium bicarbonate solution, brine, and water, dried with anhydrous magnesium sulfate, filtered, and concentrated *in vacuo* to isolate the pure product. Yield: 78.26%, Mp: 88–90 °C. ^{1}H NMR (400 MHz, DMSO-d$_6$): δ 10.47 (s, 1H), 8.64 (d, 2H), 7.15 (t, 1H), 2.47 (t, 2H), 1.56 (p, 2H), 1.27 (m, 2H), 0.86 (t, 3H). ^{13}C NMR (101 MHz, DMSO-d$_6$): δ 172.00, 158.74, 158.17, 116.99, 36.81, 31.51, 28.75, 25.12, 22.46, 14.39.

Synthesis of *N*-(pyrimidin-2-yl)octanamide (PM-heptyl). A solution of 2-aminopyrimidine (0.50 g, 5.26 mmol) in octanoic anhydride (3.13 mL, 10.52 mmol) was stirred for 1.5 h at 100 °C and then cooled to 0 °C. The precipitate that formed was filtered off, and the reaction contents were extracted from ethyl acetate. The organic layer was washed with saturated sodium bicarbonate solution, brine, and water, dried with anhydrous magnesium sulfate, filtered, and concentrated *in vacuo* to isolate the pure product. Yield: 88.79%, Mp: 95–97 °C. ^{1}H NMR (400 MHz, DMSO-d$_6$): δ 10.47 (s, 1H), 8.64 (d, 2H), 7.15 (t, 1H), 2.46 (t, 2H), 1.56 (p, 2H), 1.26 (m, 2H), 0.85 (t, 3H). ^{13}C NMR (101 MHz, DMSO-d$_6$): δ 172.02, 158.74, 158.18, 116.99, 36.81, 31.64, 29.05, 28.95, 25.17, 22.53, 14.41.

Cl-PM series

Synthesis of *N*-(5-chloropyrimidin-2-yl)acetamide (Cl-PM-methyl). A solution of 2-amino-5-chloropyrimidine (0.50 g, 3.86 mmol) in acetic anhydride (0.73 mL, 7.72 mmol) was

stirred for 1.5 h at 160 °C and then cooled to 0 °C. The precipitate that formed was washed off with hexane to get the pure product. Yield: 97.12%, Mp: 206–208 °C. ^{1}H NMR (600 MHz, DMSO-d$_6$): δ 10.76 (s, 1H), 8.74 (s, 2H), 2.16 (s, 3H). ^{13}C NMR (101 MHz, DMSO-d$_6$): δ 169.22, 156.99, 156.44, 124.70, 25.02.

Synthesis of *N*-(5-chloropyrimidin-2-yl)propionamide (Cl-PM-ethyl). A solution of 2-amino-5-chloropyrimidine (0.50 g, 3.86 mmol) in propionic anhydride (0.99 mL, 7.72 mmol) stirred for 1.5 h at 160 °C and then cooled to 0 °C. The precipitate that formed was washed off with hexane to get the pure product. Yield: 69.13%, Mp: 152–154 °C. ^{1}H NMR (600 MHz, DMSO-d$_6$): δ 10.72 (s, 1H), 8.74 (s, 2H), 2.48 (q, 2H), 1.04 (t, 3H). ^{13}C NMR (101 MHz, DMSO-d$_6$): δ 172.63, 156.96, 156.47, 124.59, 30.13, 9.55.

Synthesis of *N*-(5-chloropyrimidin-2-yl)butyramide (Cl-PM-propyl). A solution of 2-amino-5-chloropyrimidine (0.50 g, 3.86 mmol) in butyric anhydride (1.26 mL, 7.72 mmol) stirred for 1.5 h at 160 °C and then cooled to 0 °C. The precipitate that formed was washed off with hexane to get the pure product. Yield: 46.49%, Mp: 104–106 °C. ^{1}H NMR (600 MHz, DMSO-d$_6$): δ 10.72 (s, 1H), 8.74 (s, 2H), 2.44 (t, 2H), 1.58 (p, 2H), 0.90 (t, 3H). ^{13}C NMR (101 MHz, DMSO-d$_6$): δ 171.71, 156.97, 156.42, 124.67, 38.70, 18.52, 14.03.

Synthesis of *N*-(5-chloropyrimidin-2-yl)pentanamide (Cl-PM-butyl). A solution of 2-amino-5-chloropyrimidine (0.50 g, 3.86 mmol) in pentanoic anhydride (1.55 mL, 7.72 mmol) was stirred for 1.5 h at 160 °C and then cooled to 0 °C. The precipitate that formed was washed off with hexane to get the pure product. Yield: 34.15%, Mp: 101–103 °C. ^{1}H NMR (600 MHz, DMSO-d$_6$): δ 10.71 (s, 1H), 8.74 (s, 2H), 2.45 (t, 2H), 1.54 (p, 2H), 1.31 (h, 2H), 0.89 (t, 3H). ^{13}C NMR (101 MHz, DMSO-d$_6$): δ 171.85, 156.97, 156.42, 124.68, 36.52, 27.23, 22.19, 14.21.

Synthesis of *N*-(5-chloropyrimidin-2-yl)hexanamide (Cl-PM-pentyl). A solution of 2-amino-5-chloropyrimidine (0.50 g, 3.86 mmol) in hexanoic anhydride (1.79 mL, 7.72 mmol) was stirred for 1.5 h at 160 °C and then cooled to 0 °C. The precipitate that formed was washed off with hexane to get the pure product. Yield: 47.05%, Mp: 93–98 °C. ^{1}H NMR (600 MHz, DMSO-d$_6$): δ 10.70 (s, 1H), 8.74 (s, 2H), 2.44 (t, 2H), 1.54 (p, 2H), 1.27 (m, 4H), 0.86 (t, 3H). ^{13}C NMR (101 MHz, DMSO-d$_6$): δ 171.85, 156.97, 156.43, 124.67, 36.77, 31.27, 24.78, 22.36, 14.32.

Synthesis of *N*-(5-chloropyrimidin-2-yl)heptanamide (Cl-PM-hexyl). A solution of 2-amino-5-chloropyrimidine (0.50 g, 3.86 mmol) in heptanoic anhydride (2.03 mL, 7.72 mmol) was stirred for 1.5 h at 160 °C and then cooled to 0 °C. The precipitate that formed was washed off with hexane to get the pure product. Yield: 30.11%, Mp: 82–85 °C. ^{1}H NMR (600 MHz, DMSO-d$_6$): δ 10.70 (s, 1H), 8.74 (s, 2H), 2.44 (t, 2H), 1.54 (p, 2H), 1.27 (m, 6H), 0.85 (t, 3H). ^{13}C NMR (101 MHz, DMSO-d$_6$): δ 171.83, 156.97, 156.43, 124.67, 36.80, 31.50, 28.72, 25.06, 22.45, 14.39.

Synthesis of *N*-(5-chloropyrimidin-2-yl)octanamide (Cl-PM-heptyl). A solution of 2-amino-5-chloropyrimidine (0.50 g,

3.86 mmol) in octanoic anhydride (3.86 mL, 7.72 mmol) was stirred for 1.5 h at 160 °C and then cooled to 0 °C. The precipitate that formed was filtered off, and the reaction contents were extracted using chloroform. The organic layer was washed with saturated sodium bicarbonate solution, brine, and water, dried with anhydrous magnesium sulfate, filtered, and concentrated *in vacuo* to isolate the pure product. Yield: 28.28%, Mp: 87–89 °C. ^{1}H NMR (600 MHz, DMSO-d$_6$): δ 10.71 (s, 1H), 8.74 (s, 2H), 2.44 (t, 2H), 1.56 (p, 2H), 1.27 (m, 8H), 0.87 (t, 3H). ^{13}C NMR (101 MHz, DMSO-d$_6$): δ 171.85, 156.97, 156.44, 124.67, 36.80, 31.62, 29.01, 28.93, 25.10, 22.52, 14.41.

Br-PM series

Synthesis of *N*-(5-bromopyrimidin-2-yl)acetamide (Br-PM-methyl). A solution of 2-amino-5-bromopyrimidine (1.00 g, 6.00 mmol) in acetic anhydride (1.13 mL, 12.00 mmol) was stirred for 1.5 h at 150 °C and then cooled to 0 °C. The precipitate that formed was washed off with hexane to get the pure product. Yield: 89.89%, Mp: 232–234 °C. ^{1}H NMR (600 MHz, DMSO-d$_6$): δ 10.73 (s, 1H), 8.80 (s, 2H), 2.17 (s, 3H). ^{13}C NMR (151 MHz, DMSO-d$_6$): δ 169.26, 159.07, 156.65, 113.31, 25.05.

Synthesis of *N*-(5-bromopyrimidin-2-yl)propionamide (Br-PM-ethyl). A solution of 2-amino-5-bromopyrimidine (1.00 g, 6.00 mmol) in propionic anhydride (1.53 mL, 12.00 mmol) was stirred for 1.5 h at 150 °C and then cooled to 0 °C. The precipitate that formed was washed off with hexane to get the pure product. Yield: 76.38%, Mp: 162–164 °C. ^{1}H NMR (400 MHz, DMSO-d$_6$): δ 10.68 (s, 1H), 8.79 (s, 2H), 2.47 (q, 2H), 1.05 (t, 3H). ^{13}C NMR (151 MHz, DMSO-d$_6$): δ 172.66, 159.05, 156.68, 113.20, 30.16, 9.56.

Synthesis of *N*-(5-bromopyrimidin-2-yl)butyramide (Br-PM-propyl). A solution of 2-amino-5-bromopyrimidine (1.00 g, 6.00 mmol) in butyric anhydride (1.96 mL, 12.00 mmol) was stirred for 1.5 h at 150 °C and then cooled to 0 °C. The precipitate that formed was washed off with hexane to get the pure product. Yield: 79.45%, Mp: 136–138 °C. ^{1}H NMR (400 MHz, DMSO-d$_6$): δ 10.69 (s, 1H), 8.79 (s, 2H), 2.43 (t, 2H), 1.57 (p, 2H), 0.90 (t, 3H). ^{13}C NMR (151 MHz, DMSO-d$_6$): δ 173.54, 160.86, 158.45, 115.08, 40.53, 20.32, 15.85.

Synthesis of *N*-(5-bromopyrimidin-2-yl)pentanamide (Br-PM-butyl). A solution of 2-amino-5-bromopyrimidine (1.00 g, 6.00 mmol) in pentanoic anhydride (2.40 mL, 12.00 mmol) was stirred for 1.5 h at 150 °C and then cooled to 0 °C. The precipitate that formed was washed off with hexane to get the pure product. Yield: 66.52%, Mp: 116–118 °C. ^{1}H NMR (400 MHz, DMSO-d$_6$): δ 10.69 (s, 1H), 8.79 (s, 2H), 2.45 (t, 2H), 1.54 (p, 2H), 1.31 (h, 2H), 0.89 (t, 3H). ^{13}C NMR (151 MHz, DMSO-d$_6$): δ 173.69, 160.83, 158.41, 115.07, 38.33, 29.01, 13.98, 16.00.

Synthesis of *N*-(5-bromopyrimidin-2-yl)hexanamide (Br-PM-pentyl). A solution of 2-amino-5-bromopyrimidine (1.00 g, 6.00 mmol) in hexanoic anhydride (2.77 mL, 12.00 mmol) was stirred for 1.5 h at 150 °C and then cooled to 0 °C. The

precipitate that formed was washed off with hexane to get the pure product. Yield: 76.67%, Mp: 105–107 °C. ^{1}H NMR (400 MHz, DMSO-d_6): δ 10.69 (s, 1H), 8.79 (s, 2H), 2.44 (t, 2H), 1.55 (p, 2H), 1.28 (m, 4H), 0.85 (t, 3H). ^{13}C NMR (151 MHz, DMSO-d_6): δ 173.70, 160.81, 158.40, 115.05, 38.57, 35.87, 33.04, 26.56, 24.15, 16.08.

Synthesis of *N*-(5-bromopyrimidin-2-yl)heptanamide (Br-PM-hexyl). A solution of 2-amino-5-bromopyrimidine (1.00 g, 6.00 mmol) in heptanoic anhydride (3.16 mL, 12.00 mmol) was stirred for 1.5 h at 150 °C and then cooled to 0 °C. The precipitate that formed was washed off with hexane to get the pure product. Yield: 65.12%, Mp: 109–111 °C. ^{1}H NMR (400 MHz, DMSO-d_6): δ 10.69 (s, 1H), 8.79 (s, 2H), 2.44 (t, 2H), 1.55 (p, 2H), 1.28 (m, 6H), 0.86 (t, 3H). ^{13}C NMR (101 MHz, DMSO-d_6): δ 171.84, 159.05, 156.67, 113.27, 36.84, 31.51, 28.72, 25.06, 22.46, 14.40.

Synthesis of *N*-(5-bromopyrimidin-2-yl)octanamide (Br-PM-heptyl). A solution of 2-amino-5-bromopyrimidine (1.00 g, 6.00 mmol) in octanoic anhydride (3.57 mL, 12.00 mmol) was stirred for 1.5 h at 150 °C and then cooled to 0 °C. The precipitate that formed was washed off with hexane to get the pure product. Yield: 87.94%, Mp: 98–100 °C. ^{1}H NMR (400 MHz, DMSO-d_6): δ 10.68 (s, 1H), 8.79 (s, 2H), 2.44 (t, 2H), 1.55 (p, 2H), 1.26 (m, 8H), 0.85 (t, 3H). ^{13}C NMR (101 MHz, DMSO-d_6): δ 171.83, 159.04, 156.67, 113.26, 36.83, 31.63, 29.02, 28.93, 25.10, 22.53, 14.41.

Crystals suitable for single-crystal X-ray diffraction, were obtained for all 21 compounds through slow evaporation, Table 1. The **PM-methyl** crystal structure has been previously reported.[18]

Electrostatic potentials were calculated using density functional theory at the B3LYP level using the 6-311++G** basis set under vacuum, using Spartan 08' software.

Results

The calculated MEP values are shown in Fig. 4.

In each of the seven crystal structures from the **PM** series, the primary intermolecular interactions observed are a set of four hydrogen bonds, C–H(py)···O═C/N(py)···H–N/N–H···N(py)/C═O···H–C(py), which produce tightly interlocked dimers, Fig. 5.

In six out of seven structures, there is an additional C–H(py)···O═C hydrogen bond, which serves to connect adjacent dimers (it is not present in the structure of **PM-propyl**). The only other noteworthy hydrogen bonds (N(py)···H–C/C–H···N(py)) appeared in the crystal structure of **PM-methyl**, which, interestingly, is the least sterically hindered molecule in this series.

The primary noncovalent interactions in the seven crystal structures of the **Cl-PM** series are shown in Fig. 6. The addition of a halogen atom to the five-position has affected the supramolecular assembly compared to what was found in the **PM**-series. Five of the seven structures did display the dimeric features created by four complementary hydrogen bonds, C–H(py)···O═C/N(py)···H–N/N–H···N(py)/C═O···H–C(py) similar to what was found in the corresponding members of the **PM** series. However, **Cl-PM-butyl** and **Cl-PM-heptyl** were completely different and instead presented (N(py)···H–C/N–H···N(py)/C═O···H–N) and C═O···H–N interactions, respectively. Two of the seven members in this series, **Cl-PM-methyl** and **Cl-PM-propyl**, also contained halogen bonds. All but one structure, **Cl-PM-ethyl**, also displayed a secondary C–H(py)···O═C hydrogen bond. Finally, similar to what was noted in the **PM-methyl** structure, (N(py)···H–C/C–H···N(py)) were present in the **Cl-PM-methyl** structure which has the least steric hindrance in this series.

**Table 1** Solvents used for crystal growth and crystal descriptions

| Compound	Code	Solvent	Color, morphology
N-(Pyrimidin-2-yl)acetamide	**PM-methyl**	Ethyl acetate	Colorless, plate
N-(Pyrimidin-2-yl)propionamide	**PM-ethyl**	Ethyl acetate	Colorless, irregular
N-(Pyrimidin-2-yl)butyramide	**PM-propyl**	Ethyl acetate	White, needle
N-(Pyrimidin-2-yl)pentanamide	**PM-butyl**	Ethyl acetate	Colorless, irregular
N-(Pyrimidin-2-yl)hexanamide	**PM-pentyl**	Ethyl acetate	Colorless, irregular
N-(Pyrimidin-2-yl)heptanamide	**PM-hexyl**	Ethyl acetate	Colorless, needle
N-(Pyrimidin-2-yl)octanamide	**PM-heptyl**	Ethyl acetate	Colorless, needle
N-(5-Bromopyrimidin-2-yl)acetamide	**Br-PM-methyl**	Acetone + methanol	Orange, plate
N-(5-Bromopyrimidin-2-yl)propionamide	**Br-PM-ethyl**	Acetone + methanol	Orange, prism
N-(5-Bromopyrimidin-2-yl)butyramide	**Br-PM-propyl**	Acetone	Colorless, needle
N-(5-Bromopyrimidin-2-yl)pentanamide	**Br-PM-butyl**	Acetonitrile	Colorless, block
N-(5-Bromopyrimidin-2-yl)hexanamide – form 1	**Br-PM-pentyl-form 1**	Acetonitrile	Colorless, plate
N-(5-Bromopyrimidin-2-yl)hexanamide – form 2	**Br-PM-pentyl-form 2**	Acetonitrile	Colorless, plate
N-(5-Bromopyrimidin-2-yl)heptanamide	**Br-PM-hexyl**	Ethyl acetate	Colorless, needle
N-(5-Bromopyrimidin-2-yl)octanamide	**Br-PM-heptyl**	Ethyl acetate	Colorless, needle
N-(5-Chloropyrimidin-2-yl)acetamide	**Br-PM-methyl**	Ethyl acetate + acetonitrile + methanol	Colorless, irregular
N-(5-Chloropyrimidin-2-yl)propionamide	**Br-PM-ethyl**	Methanol	Colorless, irregular
N-(5-Chloropyrimidin-2-yl)butyramide	**Br-PM-propyl**	Chloroform	Colorless, plate
N-(5-Chloropyrimidin-2-yl)pentanamide	**Br-PM-butyl**	Ethyl acetate	Colorless, block
N-(5-Chloropyrimidin-2-yl)hexanamide	**Br-PM-pentyl**	Acetonitrile	Colorless, needle
N-(5-Chloropyrimidin-2-yl)heptanamide	**Br-PM-hexyl**	Ethyl acetate	Colorless, plate
N-(5-Chloropyrimidin-2-yl)octanamide	**Br-PM-heptyl**	Ethyl acetate	Colorless, needle

(a) PM Series
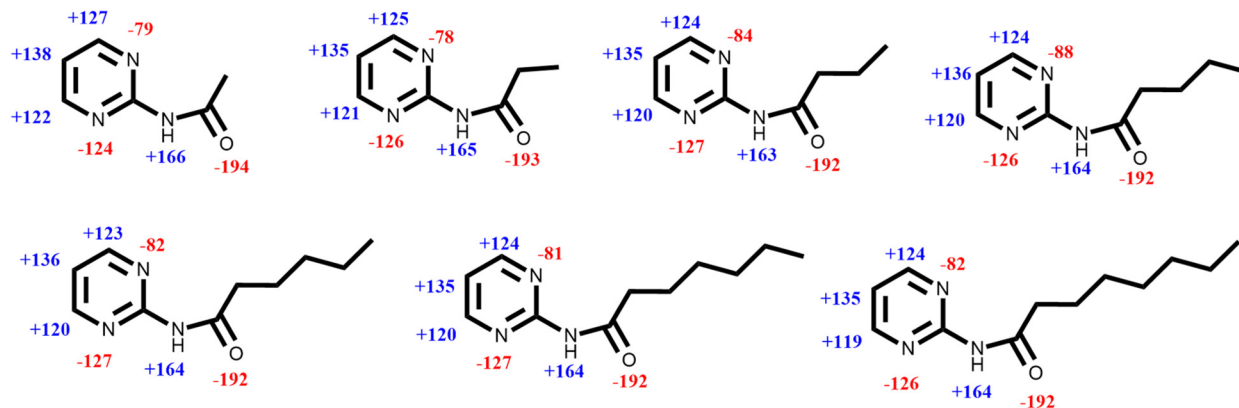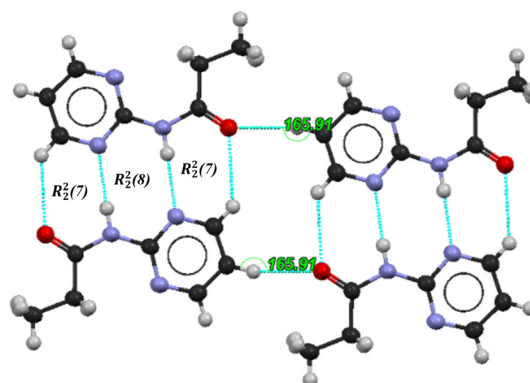
(b) Cl-PM series
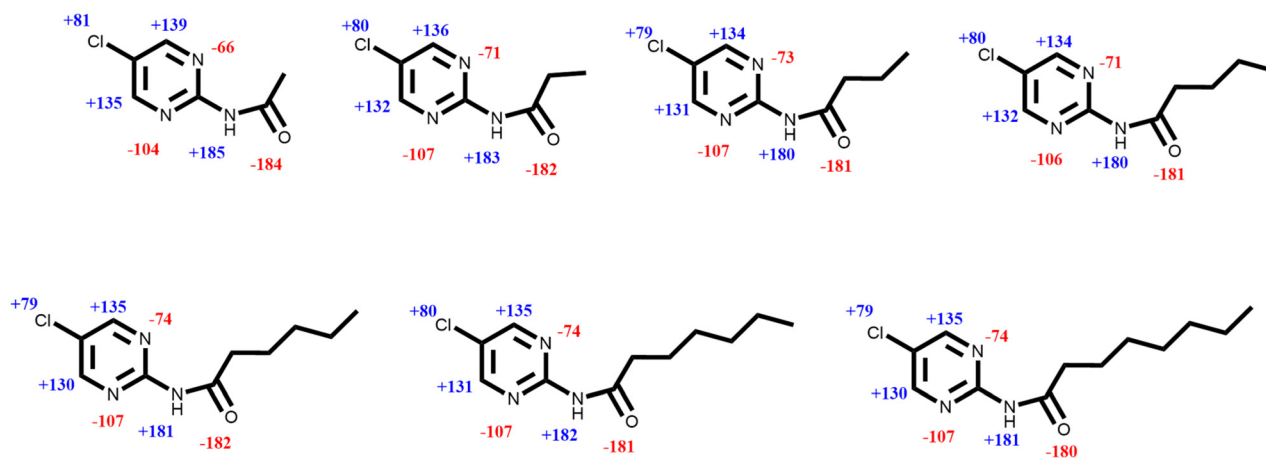
(c) Br-PM series
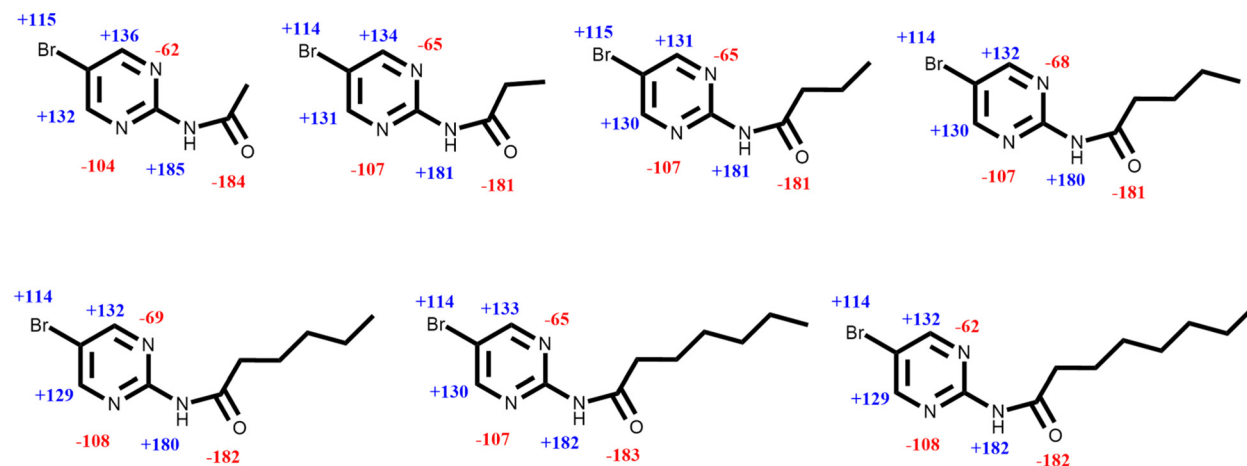
Fig. 4 MEP values (kJ mol^{-1}) at the likely donor–acceptor sites in the 21 target compounds.

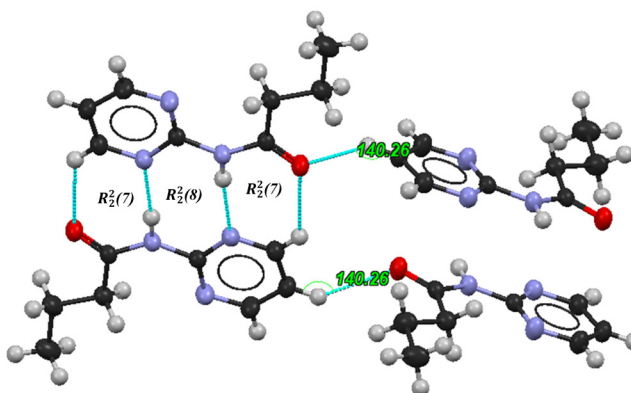(a) PM-methyl
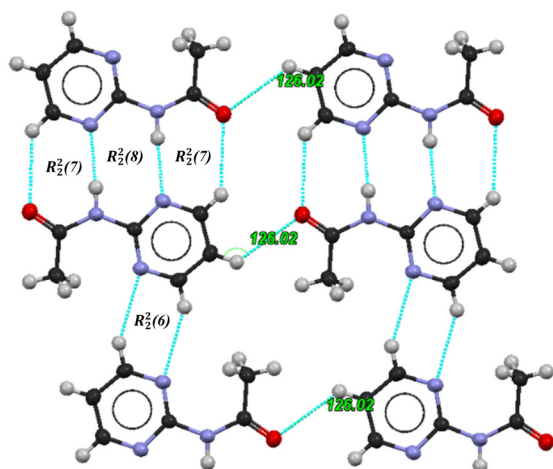
(b) PM-ethyl

(c) PM-propyl

Fig. 5 The intermolecular interactions in three different types of single crystal structures appeared in the **PM** series.

The **Br-PM** series was largely similar to the **PM** series, as all crystal structures showed the same dimers connected by four intermolecular hydrogen bonds (C–H(py)···O=C/N(py)···H–N/N–H···N(py)/C=O···H–C(py)), Fig. 7, similarly to what was found in the **PM** series. All but one structure, **Br-PM-ethyl**, also comprised a C–H(py)···O=C hydrogen bond as similar to **Cl-PM-ethyl**. Furthermore, two polymorphs of **Br-PM-pentyl** were obtained (SI). Both were crystallized from acetonitrile and appeared as colorless plates in $P\bar{1}$ and $P2_1/c$ space groups, respectively. Similar to the **PM-methyl** and the **Cl-PM-methyl** structures, an additional hydrogen bond, (N(py)···H–C/C–H···N(py)), was present in **Br-PM-methyl**, again, the least sterically hindered member in the series.

The hydrogen and halogen bond angles and distances in the 22 crystal structures are given in Table 2.

In the crystal structures, hydrogen bond angles among the inter-dimers ranged from 126° to 166°, Table 2. In the chloro series, the halogen bond angles among inter-dimers ranged from 170° to 175°, and in the bromo series, from 168°

to177°, indicating that when halogen bonds are present, they tend to be more linear than hydrogen bonds.

Discussion

We initially hypothesized that these pyrimidine derivatives would engage in four different types of synthons through N–H···O=C or N–H···N(py) hydrogen bonds, resulting in N–H···N/N···N–H, N–H···O=C/C=O···H–N homo synthons, or N···N–H/N–H···O=C, N–H···O=C hetero synthons. However, in fact only the N–H···N/N···N–H homo synthon was observed. In the final crystal structures, none of the compounds showed evidence of $C_1^1(4)$ chain formation. In contrast, additional hydrogen bonds involving aromatic protons were present in solid-state structures, resulting in self-complementary dimers assembled *via* four hydrogen bonds, Fig. 8. The aromatic protons of these molecules do carry a relatively large positive charge due to the two nitrogen atoms in the ring, allowing them to act as reasonable hydrogen-bond donors. This could also explain
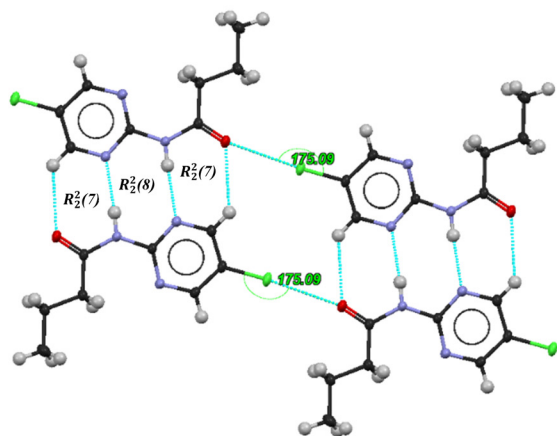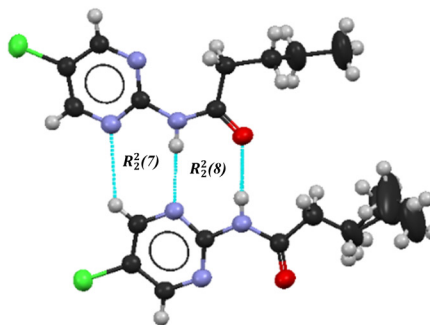
(a) Cl-PM-methyl
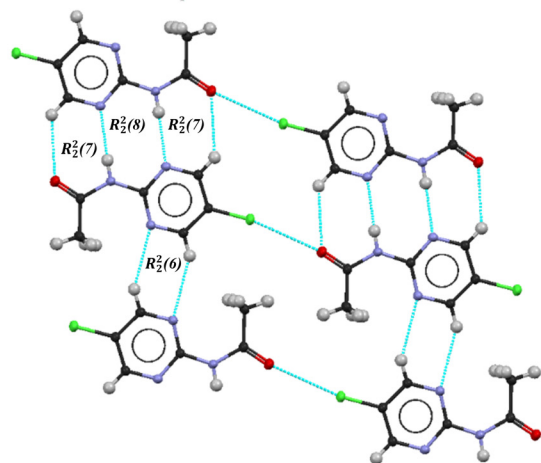
(b) Cl-PM-ethyl
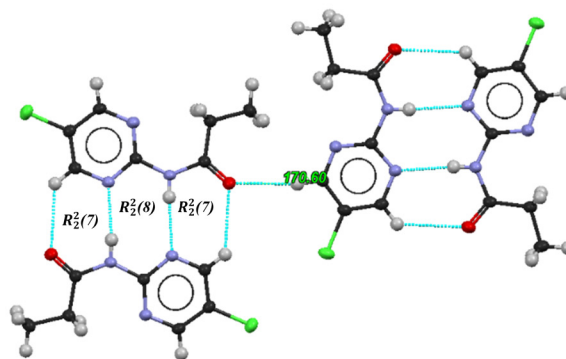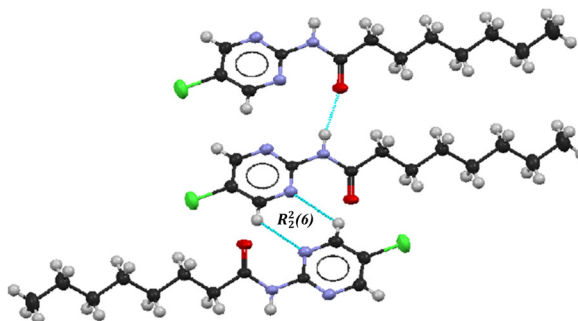
(c) Cl-PM-propyl

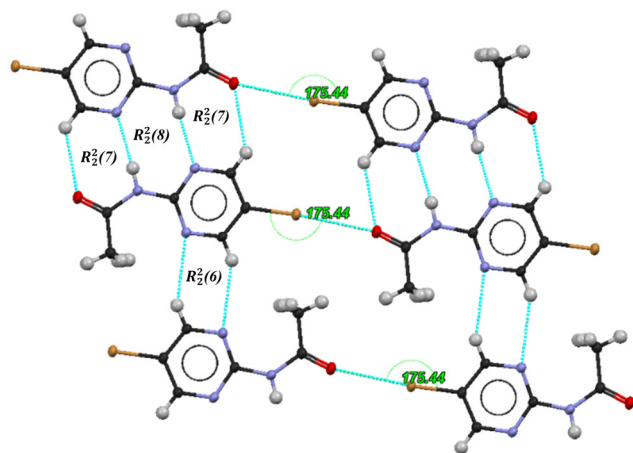(d) Cl-PM-butyl

(e) Cl-PM-heptyl

Fig. 6 The intermolecular interactions in five different types of single crystal structures appeared in the **Cl-PM** series.

how the system arranges itself in the presence of an unequal number of acceptors and donor sites. In these molecules, which conta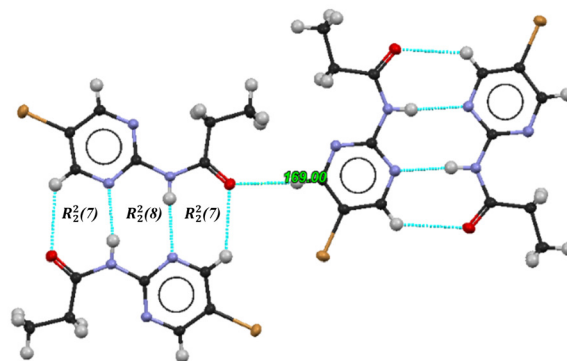in one conventional donor and three acceptors, the aromatic protons can level that imbalance by providing effective hydrogen-bond donor sites.
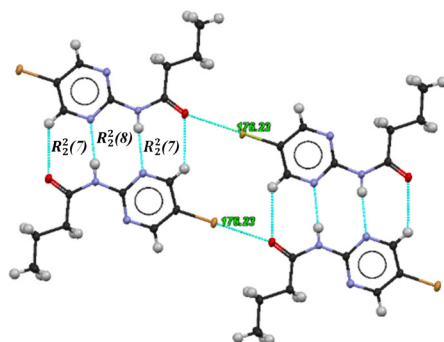
(a) Br-PM-methyl

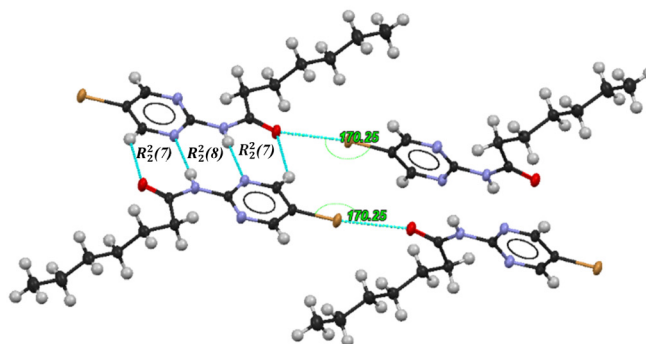(b) Br-PM-ethyl

(c) Br-PM-propyl

(d) Br-PM-hexyl

Fig. 7 The intermolecular interactions in four different types of single crystal structures appeared in the **Br-PM** series.

Table 2 Inter-dimer hydrogen or halogen bond angles and distances

Alkyl chain	PM series (hydrogen bond)		Cl-PM series (halogen bond)		Br-PM series (halogen bond)	
	C–X⋯O/°	X⋯O/Å	C–X⋯O/°	X⋯O/Å	C–X⋯O/°	X⋯O/Å
Methyl	126.02	3.348(2)	170.51	3.14998(4)	175.44	3.034(2)
Ethyl	165.91	3.226(4)	N/A	N/A	N/A	N/A
Propyl	140.26	3.184(16)	175.09	2.9322(9)	176.23	2.9105(13)
Butyl	155.68	3.4148(18)	N/A	N/A	172.06	2.8900(13)
Pentyl	156.77	3.2740(17)	N/A	N/A	176.32/172.11	2.9356(15)/2.9080(16)
Hexyl	154.71	3.294(2)	N/A	N/A	170.25	3.0090(14)
Heptyl	164.73	3.2784(17)	N/A	N/A	168.71	2.919(2)

In none of the three series did we observe any notable structural influences as a result of variations in alkyl chain lengths. The increased steric bulk and molecular 'greasiness' did not alter the primary molecular recognition events that brought adjacent molecules together into tightly bound dimeric units. Furthermore, the specific nature of the alkyl chain (odd or even number of carbon) does not produce any notable changes to the crystal structures in this series.

Generally, an increase in molecular weight tends to enhance thermal stability due to increased van der Waals forces. However, as the alkyl chain length increases, the polarity of the molecule also decreases, making the material more hydrophobic (greasy), which can also reduce thermal stability. In our case, although the molecular weight increases with the alkyl chain length, the reduction in polarity seems to be the dominant factor, leading to a decrease in thermal stability (Fig. 9). However, while chain length clearly affects thermal
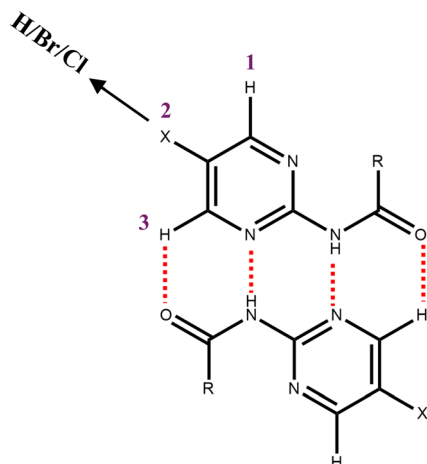
Fig. 8 The primary intermolecular interactions that were observed in 20/22 crystal structures.
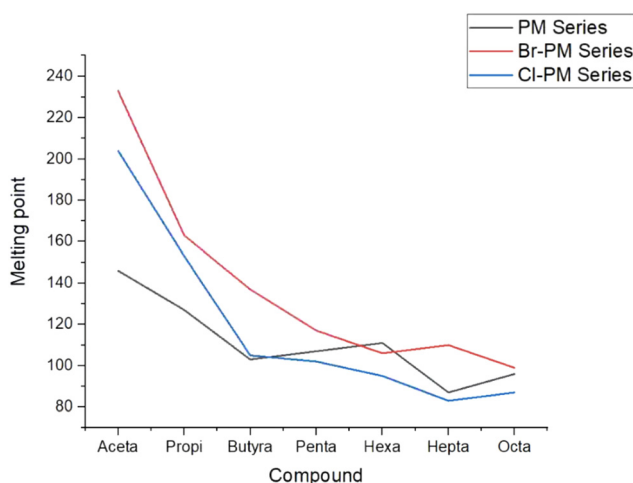

Fig. 9 Thermal stability variation of three series.

behavior, the odd or even nature of the alkyl chain shows no noticeable impact on thermal stability.

Compared to the **PM** series, the introduction of halogen atoms altered the MEP of the donor and the acceptor sites in the **Cl-PM** series and **Br-PM** series. The influence of halogen atoms decreased the acceptor potential (less negative) and increased the donor potential (more positive). The presence of electron-withdrawing groups decreases the electron density from donor sites, making them stronger donors. In contrast, the electron withdrawal from acceptor sites leads to decreased electron density, making them weaker acceptors. However, these changes in MEP did not significantly impact the supramolecular assembly, as the same primary interactions were retained in 20 out of 22 crystal structures. However, our final observations suggest that hydrogen bonds can be replaced by halogen bonds without disrupting the overall self-assembly as long as the halogen bond donor is sufficiently strong.

In this study, we synthesized three series of 2-aminopyrimidine derivates: **PM**, **Cl-PM**, and **Br-PM**. Crystal

structure determinations showed that in the **PM** series adjacent dimers were connected through C–H···O hydrogen-bond, and the other two series any inter-dimer link was provided by a near-linear halogen bond. In the **PM** series, all seven structures exhibited hydrogen bonding. In contrast, the chlorine series displayed only two halogen bonds, while in **Br-PM** a Br···O halogen bond was present in seven of eight structures (including the polymorphs). This reflects the greater polarizability of the bromine atom, which enhances its ability to participate in structure-directing halogen bonds.

In crystal structures, among the inter-dimers, hydrogen bond angles ranged from 126° to 166°, while halogen bond angles varied from 170° to 175° in the chlorine series and 168° to 177° in the bromine series. These findings highlight that halogen bonds are more directional than hydrogen bonds. In hydrogen bonds, the charge is distributed across the entire hydrogen atom on the donor site. In contrast, halogen bonds exhibit more directionality due to the specific alignment of the sigma hole along the p-orbital colinear with the covalent Cl/Br–C bond.

Conclusions

This study was motivated by an ongoing need for systematic structural investigations of amide-substituted 2-aminopyrimidine to explore the influence of, and balance between, hydrogen and halogen bonds in these crystal structures to develop a reproducible method for supramolecular reactions. We investigated 21 amide derivatives of 2-aminopyrimidine, categorized into three different series (**PM**, **Cl-PM**, and **Br-PM** series) to explore the effect of alkyl chain length, nature, and halogen substitution on supramolecular assembly. Our findings revealed that steric effects, including the alkyl chain length and whether the chain contained an odd or even number of carbons, did not influence the final crystal structures.

We observed that the same primary bonding motifs mostly remain consistent across each series. Additionally, aromatic protons were found to act as hydrogen bond donors, helping to balance systems with an unequal number of acceptors and donor sites. Moreover, we discovered that hydrogen bonds can be replaced by halogen bonds without disrupting the overall crystal assembly if the halogen bond donor is sufficiently strong enough. This was mainly observed in the bromine series, where seven out of eight structures formed halogen bonds, compared to only two out of seven in the chlorine series.

Furthermore, it was noted that halogen bonds are more directional than hydrogen bonds. This was reflected in the crystal structures, with hydrogen bond angles ranging from 126° to 166° in the **PM** series, chlorine halogen bonds varied from 170° to 175°, and bromine halogen bonds varied from 168° to 177°. Overall, these findings provide valuable insights into the role of halogen bonds in supramolecular assembly, demonstrating their potential as reliable alternatives to hydrogen bonding in crystal engineering. Understanding the

interplay between hydrogen and halogen bonds expands the possibilities of designing new molecular structures with tailored noncovalent interactions.

Conflicts of interest

There are no conflicts to declare.

Data availability

Supplementary information: the following supporting information are available free of charge. ^1H and ^{13}C NMR, FTIR spectra, DSC curves and crystallographic data. Fig. S1–S21: ^1H and ^{13}C NMR of synthesized compounds. Fig. S22–S42: FTIR spectra of all materials. Fig. S43–S63: DSC curves of all materials. Section II contains all the crystallographic data. See DOI: https://doi.org/10.1039/D5CE00839E.

Deposition numbers CCDC 2482703–2482723 contain the supplementary crystallographic data for this paper.[64a–u]

Acknowledgements

References

1 A. N. Sokolov and L. R. MacGillivray, *Cryst. Growth Des.*, 2006, **6**, 2615–2624.

2 X. Ji, J. Wang, T. Wang, N. Wang, X. Li, Y. Huang, X. Huang and H. Hao, *Ind. Eng. Chem. Res.*, 2022, **62**, 405–415.

3 M. Dergham, S. Lin and J. Geng, *Angew. Chem., Int. Ed.*, 2022, **61**, e202114267 (*Angew. Chem.*, 2022, **134**, e202114267).

4 M. T. Campos, L. S. Pires, F. D. Magalhães, M. J. Oliveira and A. M. Pinto, *Nanoscale*, 2025, **17**, 5526–5570.

5 N. Maity, M. K. Sharma, S. Ghosh, M. K. Huss-Hansen, A. Roy, R. Narayanan, M. Knaapila, W. Matsuda, S. Seki and S. Patil, *ACS Appl. Electron. Mater.*, 2023, **5**, 5093–5102.

6 H. Wang, H. K. Bisoyi, A. M. Urbas, T. J. Bunning and Q. Li, *Chem. – Eur. J.*, 2018, **25**, 1369–1378.

7 P. R. Varadwaj, H. M. Marques, A. Varadwaj and K. Yamashita, *Cryst. Growth Des.*, 2024, **24**, 7789–7807.

8 L. Meazza, J. A. Foster, K. Fucke, P. Metrangolo, G. Resnati and J. W. Steed, *Nat. Chem.*, 2012, **5**, 42–47.

9 P. Scilabra, G. Terraneo and G. Resnati, *Acc. Chem. Res.*, 2019, **52**, 1313–1324.

10 C. B. Aakeröy, M. Fasulo, N. Schultheiss, J. Desper and C. Moore, *J. Am. Chem. Soc.*, 2007, **129**, 13772–13773.

11 L. Vogel, P. Wonner and S. M. Huber, *Angew. Chem., Int. Ed.*, 2018, **58**, 1880–1891.

12 G. Haberhauer and R. Gleiter, *Angew. Chem., Int. Ed.*, 2020, **59**, 21236–21243.

13 S. Scheiner, *J. Phys. Chem. A*, 2022, **126**, 4025–4035.

14 K. T. Mahmudov, M. N. Kopylovich, M. F. C. G. da Silva and A. J. L. Pombeiro, *Dalton Trans.*, 2017, **46**, 10121–10138.

15 S. Jia, H. Ye and L. You, *Org. Chem. Front.*, 2022, **9**, 3966–3975.

16 F. Dean Toste, M. S. Sigman and S. J. Miller, *Acc. Chem. Res.*, 2017, **50**, 609–615.

17 H. Duijs, M. Kumar, S. Dhiman and L. Su, *J. Am. Chem. Soc.*, 2024, **146**(43), 29759–29766.

18 B. Ośmiałowski, E. Kolehmainen, S. Ikonen, A. Valkonen, A. Kwiatkowski, I. Grela and E. Haapaniemi, *J. Org. Chem.*, 2012, **77**, 9609–9619.

19 M. C. Aragoni, M. F. Cherchi, V. Lippolis, A. Pintus, E. Podda, A. M. Z. Slawin, J. D. Woollins and M. Arca, *Molecules*, 2022, **27**, 6289.

20 R. Bellavita, S. Braccia, A. Falanga and S. Galdiero, *Bioinorg. Chem. Appl.*, 2023, **2023**, 1–15.

21 S. T. Wu, L.-S. Long, R.-B. Huang and L.-S. Zheng, *Cryst. Growth Des.*, 2007, **7**, 1746–1752.

22 V. Caroprese, C. Tekin, V. Cencen, M. Mosayebi, N. Asmari, T. B. Liverpool, D. N. Woolfson, G. E. Fantner and M. M. C. Bastings, *Nat. Chem.*, 2025, **17**, 325–333.

23 J. M. Cameron, G. Guillemot, T. Galambos, S. Amin, E. Hampson, K. M. Haidaraly, G. N. Newton and G. Izzet, *Chem. Soc. Rev.*, 2022, **51**, 293–328.

24 E. Yashima, N. Ousaka, D. Taura, K. Shimomura, T. Ikai and K. Maeda, *Chem. Rev.*, 2016, **116**, 13752–13990.

25 F. Musil, S. De, J. Yang, J. E. Campbell, G. M. Day and M. Ceriotti, *Chem. Sci.*, 2018, **9**, 1289–1300.

26 D. R. Allan, *IUCrJ*, 2024, **11**, 438–439.

27 K. B. Ghiassi, A. J. Guenthner, N. D. Redeker, J. A. Boatz, B. G. Harvey, M. C. Davis, A. P. Chafin and T. J. Groshens, *Cryst. Growth Des.*, 2018, **18**, 1030–1040.

28 T. Endo, H. Masu, K. Fujii, T. Morita, H. Seki, S. Sen and K. Nishikawa, *Cryst. Growth Des.*, 2013, **13**, 5383–5390.

29 M. K. Corpinot and D.-K. Bučar, *Cryst. Growth Des.*, 2018, **19**, 1426–1453.

30 N. Blagden, M. de Matas, P. T. Gavan and P. York, *Adv. Drug Delivery Rev.*, 2007, **59**, 617–630.

31 O. Almarsson and M. J. Zaworotko, *Chem. Commun.*, 2004, 1889.

32 D. Tan, L. Loots and T. Friščić, *Chem. Commun.*, 2016, **52**, 7760–7781.

33 X. Niu, R. Yang, H. Zhang and J. Yang, *Adv. Agrochem*, 2022, **1**, 39–60.

34 H. Qu, Y. Gao, L. Zhou, S. Wu and J. Gong, *Chem. Eng. J.*, 2024, **490**, 151902–151902.

35 B. Sandhu, A. S. Sinha, J. Desper and C. B. Aakeröy, *Chem. Commun.*, 2018, **54**, 4657–4660.

36 S. K. Poornachary, G. Lau, P. S. Chow, R. B. H. Tan and N. George, *Cryst. Growth Des.*, 2010, **11**, 492–500.

37 Y. Ma, A. Zhang, X. Xue, D. Jiang, Y. Zhu and C. Zhang, *Cryst. Growth Des.*, 2014, **14**, 6101–6114.

38 Y. Ma, A. Zhang, C. Zhang, D. Jiang, Y. Zhu and C. Zhang, *Cryst. Growth Des.*, 2014, **14**, 4703–4713.

39 Y. Liu, T. Yu, W. Lai, Y. Ma and Z. Ge, *New J. Chem.*, 2020, **44**, 761–766.

40 Z. Yang, H. Li, X. Zhou, C. Zhang, H. Huang, J. Li and F. Nie, *Cryst. Growth Des.*, 2012, **12**, 5155–5158.

41 J. Ji, K. Wang, S. Zhu and W. Zhu, *CrystEngComm*, 2021, **23**, 2455–2468.

42 P. Yu, Y. Zhen, H. Dong and W. Hu, *Chem*, 2019, **5**, 2814–2853.

43 D. Braga, *Chem. Commun.*, 2023, **59**, 14052–14062.

44 X. L. Dai, J.-M. Chen and T.-B. Lu, *CrystEngComm*, 2018, **20**, 5292–5316.

45 S. A. Ross, D. A. Lamprou and D. Douroumis, *Chem. Commun.*, 2016, **52**, 8772–8786.

46 S. L. James, C. J. Adams, C. Bolm, D. Braga, P. Collier, T. Friščić, F. Grepioni, K. D. M. Harris, G. Hyett, W. Jones, A. Krebs, J. Mack, L. Maini, A. G. Orpen, I. P. Parkin, W. C. Shearouse, J. W. Steed and D. C. Waddell, *Chem. Soc. Rev.*, 2012, **41**, 413–447.

47 S. N. Wong, Y. Chee, B. Xuan, C. C. Sun and S. F. Chow, *CrystEngComm*, 2021, **23**, 7005–7038.

48 M. Ammar, S. Ashraf, D. A. Gonzalez-Casamachin and J. Baltrusaitis, *RSC Sustainability*, 2025, **3**, 781–803.

49 S. Cherukuvada, R. Kaur and T. N. Guru Row, *CrystEngComm*, 2016, **18**, 8528–8555.

50 S. N. Wong, M. Fu, S. Li, W. T. C. Kwok, S. Chow, K.-H. Low and S. F. Chow, *CrystEngComm*, 2024, **26**, 1505–1526.

51 P. Politzer and J. S. Murray, *Cryst. Growth Des.*, 2015, **15**, 3767–3774.

52 M. A. Spackman, J. J. McKinnon and D. Jayatilaka, *CrystEngComm*, 2008, **10**, 377–388.

53 B. Sandhu, A. McLean, A. S. Sinha, J. Desper, A. A. Sarjeant, S. Vyas, S. M. Reutzel-Edens and C. B. Aakeröy, *Cryst. Growth Des.*, 2017, **18**, 466–478.

54 B. de la Torre and F. Albericio, *Molecules*, 2018, **23**, 533.

55 B. Nammalwar and R. A. Bunce, *Pharmaceuticals*, 2024, **17**, 104.

56 L. Yet, *Privileged Structures in Drug Discovery*, 2018, pp. 237–283.

57 E. V. Koroleva, K. N. Gusak and Z. V. Ignatovich, *Russ. Chem. Rev.*, 2010, **79**, 655–681.

58 A. Siddique, S. Shaheen, A. Iftikhar, A. Faisal, H. M. Rehman, M. Shah, A. Tahir and U. Rashid, *Eur. J. Med. Chem.*, 2025, **293**, 117726.

59 W. Deng, X. Chen, K. Jiang, X. Song, M. Huang, Z.-C. Tu, Z. Zhang, X. Lin, R. Ortega, A. V. Patterson, J. B. Smaill, K. Ding, S. Chen, Y. Chen and X. Lu, *ACS Med. Chem. Lett.*, 2021, **12**, 647–652.

60 S. Xu, Y. Zhu, J. Meng, C. Li, Z. Zhu, C. Wang, Y.-C. Gu, L. Han, J. Wen, M. Tong, X. Shi, Y. Hou, Y. Liu and Y. Zhao, *Bioorg. Chem.*, 2023, **134**, 106442.

61 J. Gerninghaus, R. Zhubi, A. Kraemer, M. Karim, D. H. N. Tran, A. C. Joerger, C. Schreiber, L. M. Berger, B. T. Berger, T. A. L. Ehret, L. Elson, C. Lenz, K. Saxena, S. Mueller, S. Einav, S. Knapp and T. Hanke, *bioRxiv*, 2024, preprint, DOI: **10.1101/2024.02.18.580805**.

62 C. Mo, Z. Zhang, C. P. Guise, X. Li, J. Luo, Z. Tu, Y. Xu, A. V. Patterson, J. B. Smaill, X. Ren, X. Lu and K. Ding, *ACS Med. Chem. Lett.*, 2017, **8**, 543–548.

63 Sh. A. Kadirova, G. A. Nuralieva, M. A. Alieva, S. A. Talipov, Z. G. Tilyakov and N. A. Parpiev, *Russ. J. Gen. Chem.*, 2005, **75**, 1962–1964.

64 (*a*) CCDC 2482703: Experimental Crystal Structure Determination, 2025, DOI: **10.5517/ccdc.csd.cc2pbg6q**; (*b*) CCDC 2482704: Experimental Crystal Structure Determination, 2025, DOI: **10.5517/ccdc.csd.cc2pbg7r**; (*c*) CCDC 2482705: Experimental Crystal Structure Determination, 2025, DOI: **10.5517/ccdc.csd.cc2pbg8s**; (*d*) CCDC 2482706: Experimental Crystal Structure Determination, 2025, DOI: **10.5517/ccdc.csd.cc2pbg9t**; (*e*) CCDC 2482707: Experimental Crystal Structure Determination, 2025, DOI: **10.5517/ccdc.csd.cc2pbgbv**; (*f*) CCDC 2482708: Experimental Crystal Structure Determination, 2025, DOI: **10.5517/ccdc.csd.cc2pbgcw**; (*g*) CCDC 2482709: Experimental Crystal Structure Determination, 2025, DOI: **10.5517/ccdc.csd.cc2pbgdx**; (*h*) CCDC 2482710: Experimental Crystal Structure Determination, 2025, DOI: **10.5517/ccdc.csd.cc2pbgfy**; (*i*) CCDC 2482711: Experimental Crystal Structure Determination, 2025, DOI: **10.5517/ccdc.csd.cc2pbggz**; (*j*) CCDC 2482712: Experimental Crystal Structure Determination, 2025, DOI: **10.5517/ccdc.csd.cc2pbgh0**; (*k*) CCDC 2482713: Experimental Crystal Structure Determination, 2025, DOI: **10.5517/ccdc.csd.cc2pbgj1**; (*l*) CCDC 2482714: Experimental Crystal Structure Determination, 2025, DOI: **10.5517/ccdc.csd.cc2pbgk2**; (*m*) CCDC 2482715: Experimental Crystal Structure Determination, 2025, DOI: **10.5517/ccdc.csd.cc2pbgl3**; (*n*) CCDC 2482716: Experimental Crystal Structure Determination, 2025, DOI: **10.5517/ccdc.csd.cc2pbgm4**; (*o*) CCDC 2482717: Experimental Crystal Structure Determination, 2025, DOI: **10.5517/ccdc.csd.cc2pbgn5**; (*p*) CCDC 2482718: Experimental Crystal Structure Determination, 2025, DOI: **10.5517/ccdc.csd.cc2pbgp6**; (*q*) CCDC 2482719: Experimental Crystal Structure Determination, 2025, DOI: **10.5517/ccdc.csd.cc2pbgq7**; (*r*) CCDC 2482720: Experimental Crystal Structure Determination, 2025, DOI: **10.5517/ccdc.csd.cc2pbgr8**; (*s*) CCDC 2482721: Experimental Crystal Structure Determination, 2025, DOI: **10.5517/ccdc.csd.cc2pbgs9**; (*t*) CCDC 2482722: Experimental Crystal Structure Determination, 2025, DOI: **10.5517/ccdc.csd.cc2pbgtb**; (*u*) CCDC 2482723: Experimental Crystal Structure Determination, 2025, DOI: **10.5517/ccdc.csd.cc2pbgvc**.